Ultraviolet-visible spectroscopic characterization of lanthanum beryllate crystals doped with Pr, Nd...

Article *in* Journal of Surface Investigation X-ray Synchrotron and Neutron Techniques · January 2016

DOI: 10.1134/S1027451015060178

2 authors:

V.A. Pustovarov
Ural Federal University
299 PUBLICATIONS **995** CITATIONS

SEE PROFILE

Igor N. Ogorodnikov
Ural Federal University
197 PUBLICATIONS **840** CITATIONS

SEE PROFILE

J. Surface Investigation–X-Ray+. V.10, Is.1, January 2016, Pages 48–57. DOI: 10.1134/S1027451015060178

Ultraviolet–visible spectroscopic characterization of lanthanum beryllate crystals doped with Pr, Nd, or Er ions*

V. A. Pustovarov and I. N. Ogorodnikov
Ural Federal University, Yekaterinburg, Russia
e-mail: i.n.ogorodnikov@urfu.ru
Received June 01, 2015

Abstract—Spectroscopic characterization of lanthanum beryllate $La_2Be_2O_5$ (BLO) single crystals doped with trivalent ions of Er, Nd or Pr, was carried out in the ultraviolet-visible spectral range using synchrotron radiation spectroscopy in combination with conventional optical absorption and luminescence spectroscopy techniques. On the basis of the obtained data, the energy level diagram for these trivalent impurity ions in BLO host lattice was developed; the optical and electronic properties of the crystals were determined; the possibility of the $4f$–$4f$, $4f$–$5d$ and charge transfer transitions was analyzed; spectroscopic properties of the lattice defects formed during the introduction of trivalent impurity ions in the BLO host lattice, were investigated. We found that the lattice defects are responsible for a wide-band photoluminescence (PL) in the energy region of 400–600 nm. The most efficient excitation of the defect photoluminescence in the energy gap of BLO occurs in broad PL excitation-bands at 270 and 240 nm. The PL intensity of defects depends on the type of impurity ion and increases in the sequence: Pr–Nd–Er.

Keywords: defect-center materials, ionic crystals, laser materials, optical properties, lanthanum beryllate.
DOI: 10.1134/S1027451015060178

1. INTRODUCTION

Lanthanum beryllate single crystals $Be_2La_2O_5$ (BLO) have been the subject of intensive research after the discovery of efficient stimulated emission in BLO:Nd^{3+} [1–3], a detailed spectroscopic study of BLO:Nd^{3+} crystals in the $^4F_{3/2} \rightarrow {}^4I_{11/2,\,13/2}$ transitions [4], and the study of the laser properties (e.g. the stimulated emission cross section) of this optical material [5–7]. Pristine undoped single crystals were examined with respect to crystal structure [8], electronic structure [9], photoluminescence (PL), PL excitation (PLE) and reflection spectra [10, 11]. Studies of trivalent impurity ions in BLO crystals were performed for the impurity ions of Ce^{3+} [12, 13], Pr^{3+} [14–16] and Tm^{3+} impurity ions [17]. In 1996, the photon detector based on BLO:Ce was developed and patented [18].

It is worth noting the recent research works. Ref.[19] reports the results of a study of low-temperature (T = 10 K) reflection spectra for BLO single crystals in the energy region up to 33 eV (37.6 nm). Based on the experimental results, there were calculated spectra of the optical constants and determined the band gap E_g = 6.8 eV (182.3 nm) [19]. Luminescent-optical studies of BLO single crystals, doped with trivalent impurity ions of Ce^{3+} and Eu^{3+} were carried out in [20]. Positions of the ground $4f$ and $5d$ levels of impurity ions with respect to the levels of the BLO host crystal were determined on the basis of these experimental data [20].

Despite intensive research, many issues relating to spectroscopy of rare-earth ions in the BLO host lattice are not well understood. In particular, we are not aware of any publication on the spectroscopy of BLO:Er. The purpose of this research work is spectroscopic characterization of BLO single crystals doped with trivalent ions of Er, Nd or Pr. Firstly, we performed a spectroscopic study of rare-earth ions in BLO:Re (Re = Er, Nd, or Pr) single crystals to obtain the optical absorption spectra, the PL and PLE spectra for the energy region corresponding to transitions within the $4f$ configuration, for interconfigurational $4f$–$5d$ transitions and transitions in the vicinity of the low-energy tail of the host absorption of BLO crystal. On the basis of the obtained experimental data and semi-empirical model proposed by P. Dorenbos [21], the energy level diagram for these trivalent impurity ions in the BLO host lattice has been developed. The possibility of the $4f$–$4f$, $4f$–$5d$ and charge transfer (CT) transitions were analyzed for BLO single crystal.

Secondly, we used these results to evaluate the spectroscopic contribution from lattice defects. A synchrotron radiation spectroscopy was used at this stage to excite the luminescence of defects and recording PLE spectra. Although the experimental technique used does not allow us to identify the origin of the lattice defects, we identified a spectroscopic 'portrait' of these defects, which provide us with relevant information for future practical applications of this compound.

* The article is published in the original.

Postprint published online *December 15, 2015*

2. EXPERIMENTAL DETAILS

All the examined BLO single crystals of optical quality were grown by V.N. Matrosov using Czochralski method at the Institute of Geology and Geophysics of SB RAS (Novosibirsk, Russia). Crystal growth details have been described in [22]. The grown crystals were inspected by X-ray techniques, and results of these studies have been published previously as separate papers. It is worth noting several few important papers in this series. Tsvetkov et al. [22] have studied BLO single crystals using methods of transmission X-ray topography, X-ray powder diffraction, and X-ray microprobe analysis. The main conclusion of Ref.[22] was formulation of the conditions for growing BLO single crystals having a minimum quantity of structural defects. In this connection, we would like to mention two important facts. Firstly, all the crystals reported in our study are grown under the conditions formulated in Ref. [22]. Secondly, crystallographic parameters of the grown crystals are in agreement with [8].

We used single crystals of lanthanum beryllate: pristine undoped (BLO), doped with trivalent impurity ions of erbium (BLO:Er, 0.15 at%), neodymium (BLO:Nd, 0.15 at%), and praseodymium (BLO:Pr, 0.5 at%). It is worth noting that all dopant concentrations have been given for raw materials in the melt. Samples in the form of the polished optical quality discs (10–15 mm in diameter, 0.3–1.0 mm thick) were prepared for spectroscopic studies.

The broad-band PL emission and excitation spectra in the UV-visible spectral region were recorded at the SUPERLUMI experimental station of HASYLAB [23] upon selective photoexcitation with synchrotron radiation. The primary 2 m-vacuum monochromator equipped with two in situ interchangeable gratings, Al and Pt coated, had a typical resolution of 0.32 nm. The PLE spectra were corrected to an equal number of incident photons using sodium salicylate—a luminophore with the energy-independent quantum yield over the studied spectral range. The 0.3 m ARC Spectra Pro-300i monochromator equipped with an R6358P (Hamamatsu) photomultiplier tube was used as a registration system. The measurements were performed at $T = 80$ and 290 K using a continuous-flow cryostat mounted in the ultra-high vacuum chamber with a pressure of residual gases lower than 1×10^{-8} Pa.

The 3 m DFS-13 high-resolution diffraction spectrograph with inverse linear dispersion of 2 Å/mm was used to record PL emission spectra of the narrow spectral lines from $4f$–$4f$ transitions. Ultrahigh-pressure xenon lamp DKSSh-1000 was used as the excitation source. In other cases, PL and PLE spectra in the spectral range of 200–1000 nm were recorded using a MDR-23 type monochromator and a R6358-10 (Hamamatsu) type photoelectron multiplier tube. In this case, a 400 W deuterium discharge lamp (DDS-400) and the primary double-prism monochromator (DMR-4) were used for PL excitation. All PLE spectra are normalized to an equal number of photons incident on the sample, using a sodium salicylate—luminophore with a unit quantum yield in the energy range studied.

Optical absorption spectra were recorded at room temperature by the means of a Heλios Alpha 9423UVA1002E spectrophotometer ($\lambda = 190$–1000 nm) equipped with the Vision 32 software. The narrow spectral lines in the absorption spectra of $4f$–$4f$ transitions were recorded at $T = 80$ K by means of a streamlined BECKMAN UV-5270 spectrophotometer. Linear optical absorption coefficient α was calculated using the formula $\alpha = -\ln(\tau)/l$, where τ is an optical transmittance, l is a sample path-length.

3. RESULTS AND DISCUSSION

3.1. Energy Level Diagram

Electronic structure of lanthanide ions (Ln) in the Free State is well known, studied in detail and its description can be found in numerous publications and monographs, see e.g. [24]. The $4f$ inner shells of lanthanide ions are well shielded from external influences. Electronic energy structure of $4f$ states is described by the extended Dieke diagram [25]. When placing the ion into the host crystal, the positions of $4f$-levels with respect to the ground state change within no more than 100 cm^{-1} (about 0.01 eV). In this regard, the characterization of $4f$ ion states in most cases requires only determination of the location of its $4f^n$-ground state with respect to the host crystal (where n is the number of $4f$-electrons). Energy level diagram (Fig. 1) was constructed on the basis of two information sources. Firstly, the energy locations for $4f$ and $5d$ ground stats for all divalent and trivalent lanthanide ions in the lanthanum beryllate host lattice have been calculated in our previous work [20]. The calculation [20] was carried out in the framework of semi-empirical model proposed by P. Dorenbos. Our own experimental data on spectroscopy of BLO:Ce and BLO:Eu were used there as reference. All relevant details regarding the semi-empirical model can be found in [21]. Secondly, the Dieke diagram [25] was used to characterize the energy locations of other $4f$ levels with respect to $4f$ ground state. Let us discuss in more detail the energy level diagram, Fig. 1.

Er^{3+} ion. The $4f^{11}$ ground state of Er^{3+} ion ($^4I_{15/2}$) is located in the valence band (VB) at 1.26 eV below the VB top of BLO crystal. Optical transparency band of BLO crystal covers only intraconfiguration $4f$–$4f$ transitions from the ground $^4I_{15/2}$ state onto the excited $4f$ states up to $^4D_{3/2}$ states. The calculated en-

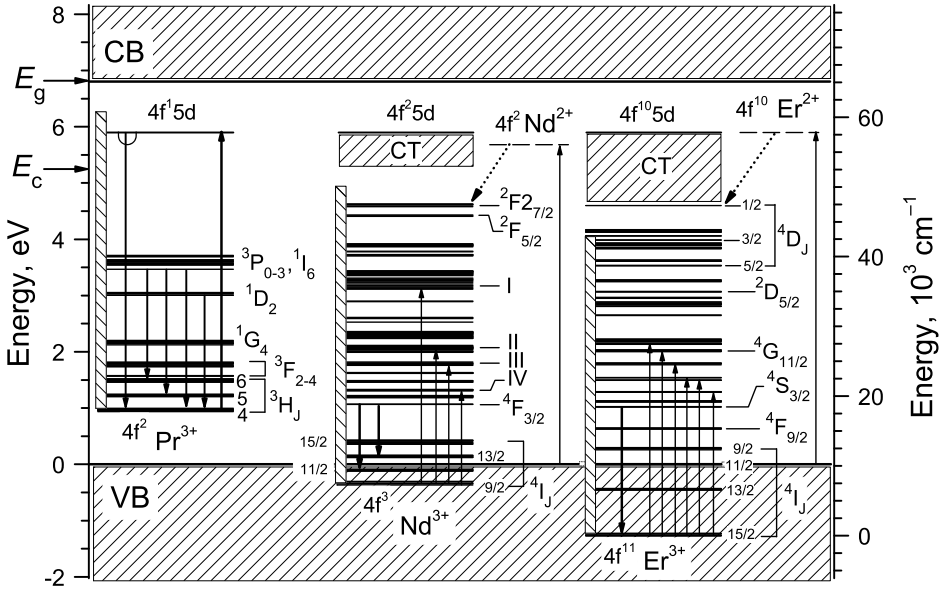

Figure 1. The calculated energy level diagram for the Pr^{3+}, Nd^{3+} and Er^{3+} ions in BLO single crystal. The arrows correspond to E_c and E_g energy values. The shaded bar represents the energy range of BLO transparency for the analysis of $4f$–$4f$ transitions. Roman numerals correspond to certain energy levels of Nd^{3+}: (I) $^4D_{3/2}$ + $^4D_{5/2}$; (II) $^4G_{9/2}$ + $^2K_{13/2}$ + $^4G_{7/2}$; (III) $^4G_{5/2}$ + $^2G_{7/2}$; (IV) $^4F_{7/2}$ + $^4S_{3/2}$.

energy values for interconfigurational $4f^{11} \rightarrow 5d\,4f^{10}$ transition (7.2 eV) and CT transition O–Er (5.9 eV) fall in the energy range of the BLO host absorption. absorption.

Nd^{3+} ion. The $4f^3$ ground state of Nd^{3+} ion ($^4I_{9/2}$) is located in the valence band at 0.36 eV below the VB top of BLO crystal. Optical transparency band of BLO crystal covers only intraconfiguration $4f$–$4f$ transitions from the ground $^4I_{9/2}$ state onto the excited $4f$ states up to $^2F2_{7/2}$ states. The calculated energy values for interconfigurational $4f^3 \rightarrow 5d\,4f^2$ transition (6.25 eV) and CT transition O–Nd (5.68 eV) fall in the energy range of the BLO host absorption.

Pr^{3+} ion. The $4f^2$ ground state of Pr^{3+} ion ($^3H_4$) is located in the band gap at about 1 eV above the VB top in BLO crystal. The optical transparency band of BLO crystal covers the following optical transitions from the ground $^3H_4$ state. Firstly, intraconfigurational $4f$–$4f$ transitions onto excited $4f$-levels up to ^3P_J, $^1I_6$ states. Secondly, interconfigurational $4f^2 \rightarrow 5d\,4f^1$ transitions with the expected energy threshold in the energy range of 4.5–4.8 eV. It is worth noting that the $^1S_0$ state is located at 1.5 eV above the $5d\,4f^1$ energy level. In this regard, a hypothetical transition to 1S0 level will be completely overwhelmed by much more intense $4f$–$5d$ transitions. In addition, the expected energy of $^3H_4 \rightarrow {}^1S_0$ transition is about 5.83 eV, which corresponds to the energy range of the BLO host absorption (bandgap E_g = 6.8 eV according to Ref.[19]). In this regard, we could not expect a manifestation of this state in the optical spectra of BLO:Pr.

It is worth noting that the synchrotron radiation VUV-spectroscopy method would be really beneficial for constructing the energy diagrams as the experimental spectra would be a direct proof of the proposed level schemes. Early results on synchrotron radiation spectroscopy for BLO:Pr are reported in [26]. We have also started such a research work for BLO:Ln^{3+} single crystals [27], but it is still premature to discuss these results.

In spite of the approximate nature of the developed energy-level diagram (Fig. 1), it has been very useful for the interpretation of the experimental data.

3.2. Optical Absorption Spectroscopy

Figure 2 shows the optical absorption spectra recorded at 290 K in the energy region near the low-energy tail of the BLO host absorption. Calculated spectrum of the Urbach tail of the BLO host absorption is drawn using the Urbach tail parameters reported in [19]. This spectrum is shown for comparison and indicates the cutoff energy E_c = 5.25 eV (236.2 nm) for T = 290 K, Fig. 2 (curve *1*). Optical absorption spectrum for pristine undoped BLO crystal (Fig. 2, curve *2*) is red-shifted by about 20 nm in comparison with the calculated spectrum. This indicates the presence of unidentified defects that determine the optical absorption near the host absorption edge. Optical absorption spectrum for BLO:Nd crystal (Fig. 2, curve *3*) is similar to the previous spectrum, but the magnitude of the red-shift with respect to the

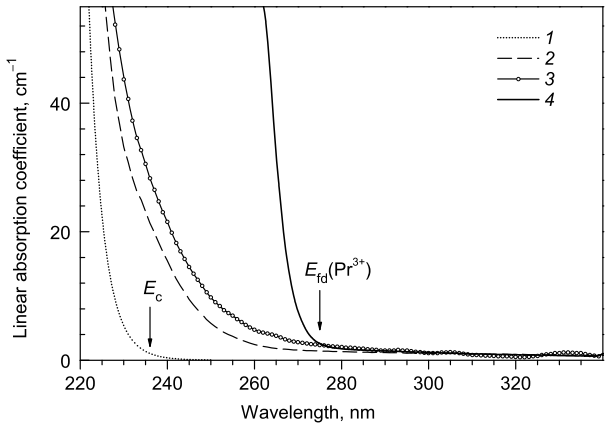

Figure 2. Absorption spectra of lanthanum beryllate single crystals. Experimental data recorded at $T = 290$ K for: (2) pristine undoped BLO; (3) BLO:Nd^{3+} (0.15 at%); (4) BLO:Pr^{3+} (0.5 at%); Dotted line (*1*) shows the Urbach tail of the host absorption calculated using the Urbach tail parameters reported in Ref.19 The arrows correspond to E_c and E_{fd} (Pr^{3+}) values in the wavelength scale.

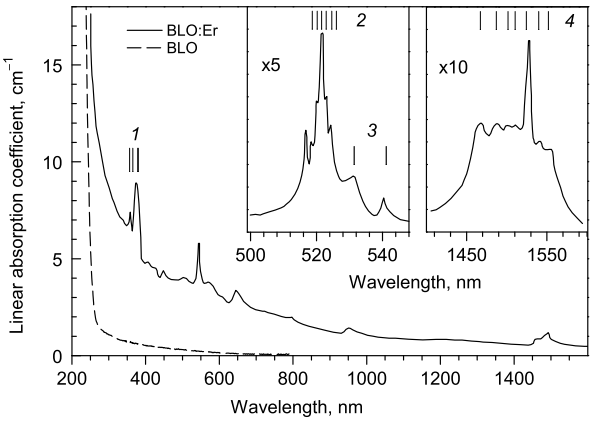

Figure 3. Absorption spectra of BLO:Er^{3+} (0.15 at%) single crystal. Inserts show (in an enlarged scale) the absorption spectra in the energy region of $4f$–$4f$ transitions. A possible interpretation of the spectral lines is shown: (1) $^4I_{15/2} \rightarrow {}^4G_J$ (J= 7/2–11/2); (2) $^4I_{15/2} \rightarrow {}^2H_{11/2}$; (3) $^4I_{15/2} \rightarrow {}^4S_{3/2}$; (4) $^4I_{15/2} \rightarrow {}^4I_{13/2}$. Dashed line shows the optical absorption spectrum of pristine undoped BLO crystal.

calculated spectrum is estimated at about 30 nm. This indicates that the introduction of Nd^{3+} impurity in the BLO host lattice is accompanied by the formation of additional lattice defects that determine the optical absorption in the spectral range of 240–280 nm (4.4–5.2 eV). Optical absorption spectrum of BLO:Pr crystal (Fig. 2, curve *4*) differs fundamentally from the previous cases: at energies above the energy threshold $E_{fd} = 4.5$ eV (274 nm), a steep increase in the optical absorption due to $4f^2 \rightarrow 5d\,4f^1$ transitions is observed there.

Figure 3 shows the optical absorption spectra of BLO:Er, recorded at 290 K in comparison to those of pristine undoped BLO crystal. From Fig. 3 it is evident that optical absorption of BLO:Er decreases gradually in the entire investigated spectral range from the shortest wavelength corresponding to E_c up to 1.5 μm. This may indicate the formation of a significant amount of defects caused by the introduction of erbium dopant in BLO host lattice. Groups of narrow lines due to $4f$–$4f$ optical transitions in Er^{3+} ion are observed on the background of gradually decreasing curve. Figure 3 also shows the identification of lines for transitions from the $^4I_{15/2}$ ground state onto the $4f$ excited states. Survey spectrum shows transitions onto the ^4G_J (J= 7/2, 9/2, 11/2) states, whereas transitions onto the $^2H_{11/2}$, $^4S_{3/2}$, $^4I_{13/2}$ states are shown in the insets in an enlarged scale.

The $4f$–$4f$ absorption spectra of BLO:Nd have also been studied in a spectral range up to E_c. The spectra are consistent with previously published data on BLO:Nd^{3+} [1–3]. In this regard, Fig. 4 shows only a fragment of UV–VIS spectrum for BLO:Nd, which consists of several series of the lines caused by $4f$–$4f$ transitions in Nd^{3+}. The most intense groups of the optical absorption lines in Fig. 4 correspond to electronic transitions from the $^4I_{9/2}$ ground state onto the excited states of $^4D_{3/2}$ + $^4D_{5/2}$ (350–365 nm), $^4G_{9/2}$ (510 nm), $^2K_{13/2}$ + $^4G_{7/2}$ (530 nm), $^4G_{5/2}$ + $^2G_{7/2}$ (570–590 nm), $^4F_{7/2}$ + $^4S_{3/2}$ (730–750 nm).

Figure 5 shows the optical absorption spectra recorded for BLO:Pr at 290 K in the energy range of $4f$–$4f$ transitions. The spectrum shows the interpretation of the lines corresponding to the $^3H_4 \rightarrow {}^3P_J$, $^3H_4 \rightarrow {}^1D_2$, $^3H_4 \rightarrow {}^3F_{3,4}$, and $^3H_4 \rightarrow {}^3H_6$ transitions in Pr^{3+} ion.

3.3. PL Emission and PL Excitation Spectra of Ln^{3+} Ions

Er^{3+} ion. The calculated values of the energy thresholds for interconfigurational $4f$–$5d$ transitions and charge-transfer transitions O–Er are located in

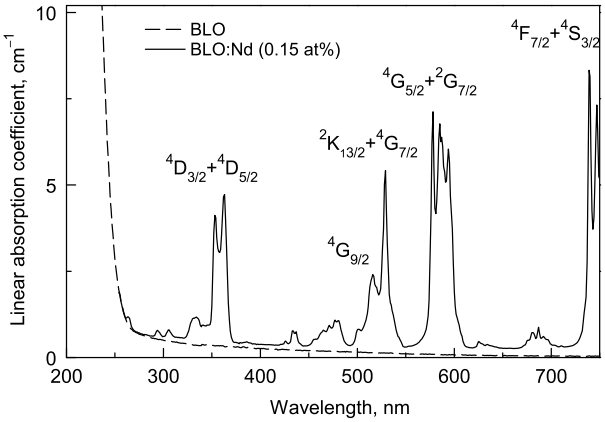

Figure 4. Absorption spectra of BLO and BLO:Nd^{3+} (0.15 at%) single crystals in the UV-VIS spectral region.

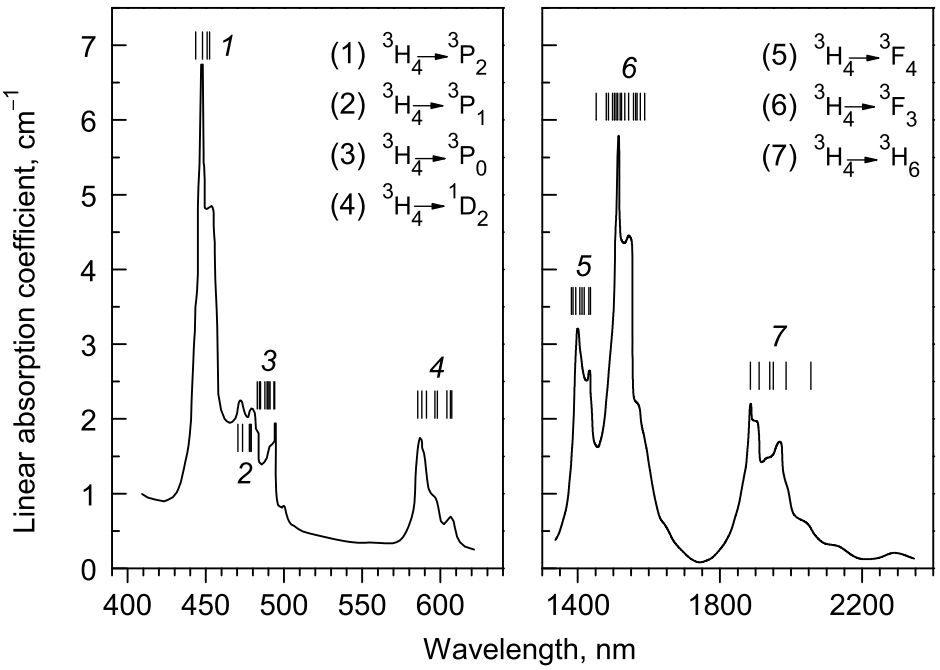

Figure 5. Absorption spectra of BLO:Pr^{3+} (0.5 at %) single crystal recorded at $T = 290$ K in the energy range of $4f$–$4f$ transitions. A possible interpretation of the spectral lines is shown.

the energy range of the BLO host absorption, Fig. 1. In this connection, we can expect to observe only the luminescence due to $4f$–$4f$ transitions.

Figure 6a shows PL emission spectra recorded for BLO:Er crystal (0.15 at %). The BLO:Er luminescence occurs in the green spectral region. It is due to radiative transitions from the $^4S_{3/2}$ level onto the sublevels of the $^4I_{15/2}$ ground multiplet, there are nine lines. At $T = 80$ K, the spectrum was dominated by the 553.6 nm line corresponding to the transition from the $^4S_{3/2}$ level onto a Stark component of $^4I_{15/2}$. The half-width of the line at $T = 80$ K is 1.3 nm. When we change the temperature from 290 to 80 K, the luminescence intensity increases significantly, the lines become narrower, the resolution becomes better that allows us to distinguish between the Stark splitting sublevels of $^4I_{15/2}$. Splitting value for $^4I_{15/2}$ level is negligible and it is about 100 cm^{-1}.

Characteristic line-like spectrum of the $4f$–$4f$ luminescence in BLO:Er appears against the background of a relatively broad PL emission band at 540–565 nm, which should be attributed to lattice defects. In contrast to the $4f$–$4f$ luminescence, the defect luminescence exhibits increased intensity at $T = 290$ K. On cooling to $T = 80$ K, the defect luminescence decreases markedly in intensity.

Figure 6b shows PLE-spectra in the region of 350–500 nm recorded for BLO:Er (0.15 at %). From Fig. 6b, it follows that there are seven narrow bands due to direct selective photoexcitation of Er^{3+} ion through electronic transitions from the $^4I_{15/2}$ ground state onto the excited states of $4f^{11}$ configuration. The most intense PLE-lines are due to electronic transitions onto the following excited state: $^2K_{15/2}$, $^4G_{11/2}$, $^2G_{9/2}$, $^4F_{3/2}$, $^4F_{5/2}$, and $^4F_{7/2}$.

Nd^{3+} ion. The situation is similar to the previous case. From the energy level diagram (Fig. 1) it follows that the calculated values of the energy thresholds for $4f$–$5d$ transitions and CT transitions O–Nd are located in the energy range of the BLO host absorption. In this regard, only the $4f$–$4f$ luminescence of Nd^{3+} can be expected for BLO:Nd. We have measured $4f$–$4f$ emission due to transitions within the $4f^3$ configuration of Nd^{3+} in BLO:Nd. Our results were in agreement with published data of [1, 3, 4]. In this regard, we do not present experimental data on the PL and PLE spectra for the $4f$–$4f$ luminescence in BLO:Nd crystals, focusing on the next section.

Pr^{3+} ion. Figure 7a shows PL spectra recorded for BLO:Pr (0.15 at %) at $T = 80$ and 290 K and $\lambda_{ex} = 253$–264 nm. The spectral profile in the energy range from 275–430 nm consists mainly of broad doublet bands with maxima at 359 and 302 nm (27800 and 33250 cm^{-1}). The main part of the PL spectrum is due partially allowed radiative transitions from the lowest excited state of $4f^1\,5d$ configuration onto the $^3H_{4,5,6}$ and $^3F_2$ states of $4f^2$ configuration. The shape of the spectrum is preserved for all specified measurement conditions. However, the PL intensity is highest at $T = 290$ K. Upon cooling to $T = 80$ K, the PL intensity is about 60% of that at room temperature. This is quite consistent with complicate temperature behavior of d–f emission in (Ba, Ca, Sr)F_2:Pr [28].

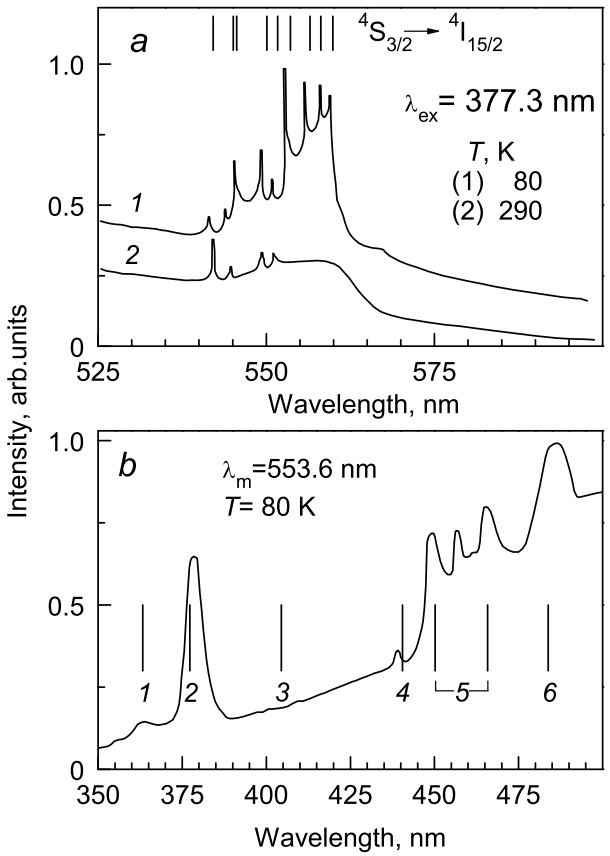

Figure 6. Photoluminescence spectra of BLO:Er^{3+} single crystals recorded with spectral resolution of 0.8 nm. Panel (a) shows PL emission spectra recorded at T= 80 and 290 K upon excitation at λ_{ex}. Panel (b) shows PLE spectra recorded at T= 80 K monitoring emission at λ_m. Possible assignments were shown for $4f$–$4f$ transitions from the $^4I_{15/2}$ ground state onto the excited states: (1) $^2K_{15/2}$, (2) $^4G_{11/2}$, (3) $^2G_{9/2}$, (4) $^4F_{3/2}$, (5) $^4F_{5/2}$, and (6) $^4F_{7/2}$.

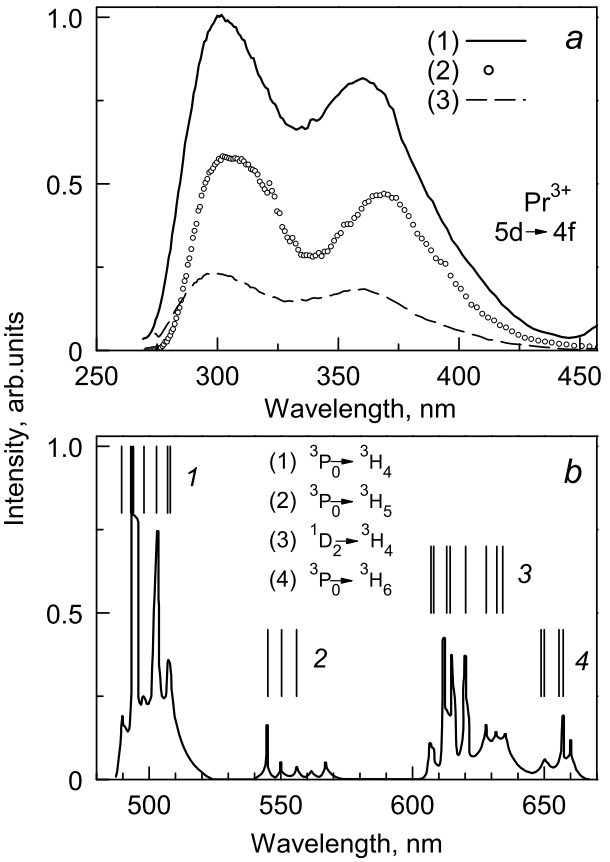

Figure 7. PL emission spectra of BLO:Pr^{3+} single crystals. Panel (a) shows the d–f emission spectra recorded at T= 80 (*2*) and 290 K (*1*, *3*) upon excitation at λ_{ex}= 264 nm (3), 259 nm (*1*) and 253 nm (*2*). Panel (b) demonstrates the f–f emission spectrum recorded at T= 80 K with spectral resolution of 0.8 nm upon excitation at λ_{ex}= 450 nm. Possible assignments for radiative transitions (*1–4*) were shown.

It is worth noting that our data are consistent mainly with the results obtained upon excitation of BLO:Pr crystal by 265 nm-laser pulses (CW laser Ar^+), where they found the locations of the doublet peaks at 28000 and 34000 cm^{-1} [15].

Figure 7b shows PL spectrum of BLO:Pr (0.5 at %) recorded with a spectral resolution of 0.8 nm at T= 80 K and λ_{ex}= 450 nm. Groups of narrow lines are due to $4f$–$4f$ transitions in Pr^{3+} ions. The most intense PL lines are due to the $^3P_0 \rightarrow {}^3H_{4,5,6}$ and $^1D2 \rightarrow {}^3H_4$ radiative transitions within $4f^2$ configuration.

Figure 8a shows PLE-spectra recorded for BLO:Pr (0.5 at %) at T= 80 and 290 K monitoring emission at 302 nm. PLE-spectrum at T= 80 K is represented by a wide asymmetric peak with a maximum at 250–253 nm (39500—39900 cm^{-1}). The high-energy slope of the PLE band is represented by a curve that gradually decreases from a maximum to a minimum value at 210–214 nm. It is worth noting that the high-energy part of this band falls into the host absorption energy range of BLO: E_c= 5.25 eV (236 nm) at 290 K and 5.49 eV (225 nm) at 80 K. The d–f emissions of BLO:Ln^{3+} (Ln= Er, Nd, Pr) are not efficiently excited in the host absorption energy range. This is quite consistent with earlier studies of d–f emission in $LiYF_4$:Er crystals [29]. Low-energy slope of the PLE band is represented by rapidly falling curve that corresponds to the energy threshold for the $4f$–$5d$ transitions in BLO:Pr crystal at T= 80 K (E_{fd}= 4.5 eV or 275 nm). At room temperature, the low-energy slope is subject to the 0.13 eV red-shift. A possible reason for this shift may be the presence of lattice defects induced by the introduction of Pr^{3+} dopant. A detailed discussion will be done in the next Section, together with a discussion of Fig. 10c.

Figure 8b shows PLE-spectra recorded in the UV energy range of 210–350 nm for BLO:Pr (0.5 at %) at 290 K monitoring emissions of different lines at 355–620 nm. These PL lines correspond to $4f$–$4f$ transitions in Pr^{3+} ion. The PLE-spectra of all luminescence

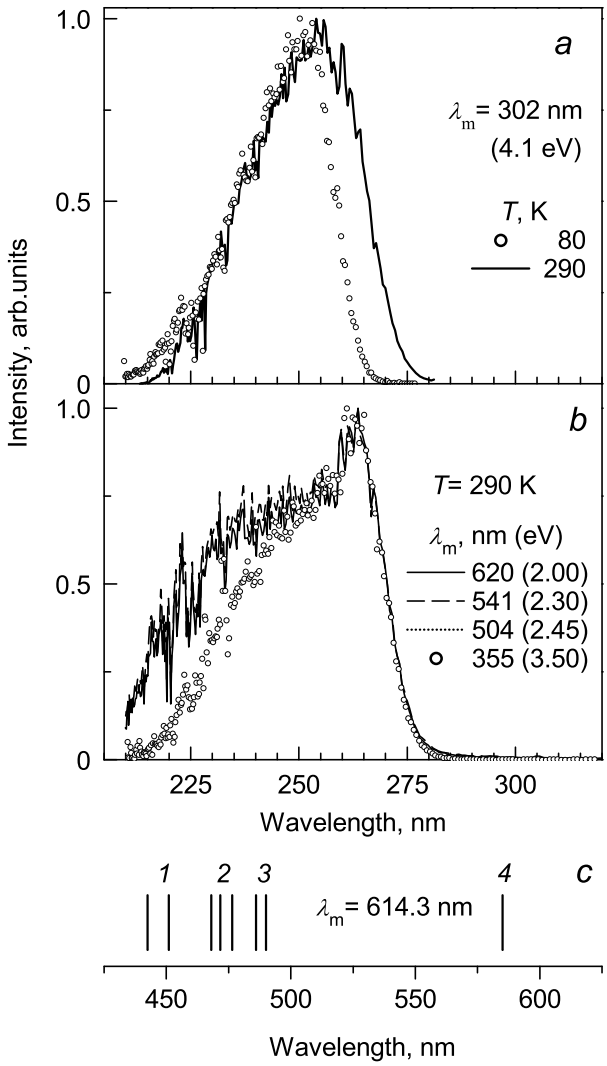

Figure 8. PL excitation spectra of BLO:Pr^{3+} single crystals recorded at $T = 80$ and 290 K monitoring emission at $\lambda_m = 302$ nm (a) and λ_m (b). Panel (c) shows spectral positions of the PL excitation lines for $4f$–$4f$ transitions from the $^3H_4$ ground state onto the excited states: (1) $^3P_2$, (2) $^3P_1$, (3) $^3P_0$, and (4) $^1D_2$ recorded monitoring emission at 614.3 nm.

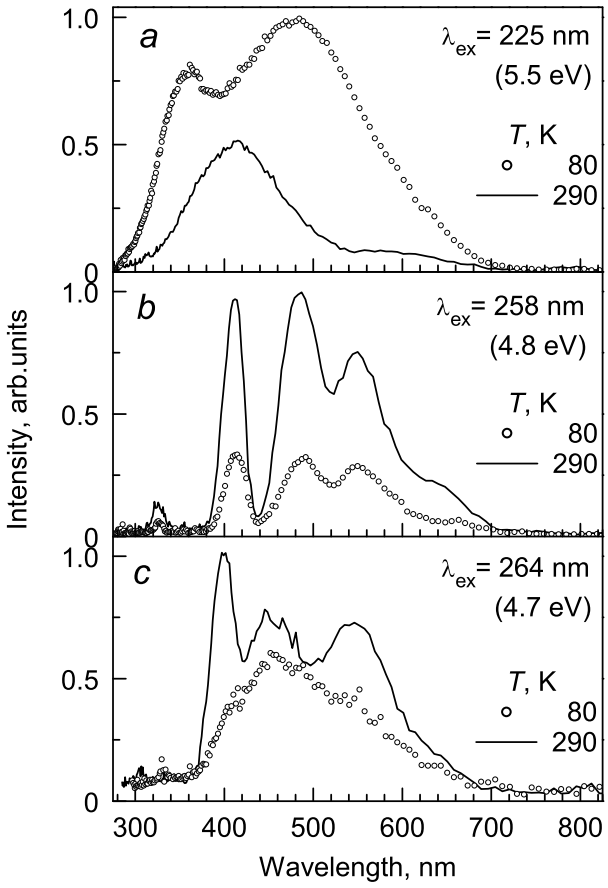

Figure 9. PL emission spectra of lanthanum beryllate single crystals recorded at $T = 80$ and 290 K upon UV-excitation at λ_{ex}. Panel (a) shows the spectra for pristine undoped BLO crystal. Panels (b, c) demonstrate spectra for BLO crystals doped with Er^{3+} (b) or Nd^{3+} (c). Spectra of each Panel are normalized to the maximum, but they are comparable in intensity with each other within the Panel.

lines registered monitoring emission at 355–620 nm, are the same. In the UV spectral range, PLE-spectra of $4f$–$4f$ luminescence are mainly the same as PLE-spectrum of $5d$–$4f$ luminescence. The slight difference is that in the 213–258 nm spectral region, PLE spectra for $4f$–$4f$ emission have a higher intensity in comparison with that for $5d$–$4f$ luminescence, Fig. 8b.

In the visible spectral region, we also measured the PLE-spectra, recording the emission at different lines corresponding to the $4f$–$4f$ radiative transitions. These spectra are identical under the condition $\lambda_{ex} < \lambda_m$. In addition, they are consistent with previously obtained data for PLE-spectra in the visible spectral region recorded for BLO:Pr monitoring $4f$–$4f$ emission [4, 14, 15]. In this context, we present the results for only one spectrum. Figure 8c shows the spectral position of PLE-lines recorded for BLO:Pr crystal at $T = 80$ K monitoring emission at 614.3 nm. The PLE-line in the spectrum correspond to intra-configurational transitions from the $^3H_4$ ground state onto the excited $^3P_2$, $^3P_1$, $^3P_0$ and $^1D_2$ state of Pr^{3+} ion.

3.4. *Spectroscopic Manifestation of Defects in BLO*

Optical absorption spectra (Figs. 2–4 for BLO:Er, BLO:Nd) and PLE-spectra (Fig. 8 for BLO:Pr) provide experimental evidence for spectroscopic manifestation of lattice defects in BLO single crystals.

Figure. 9a shows PL emission spectra for the pristine undoped BLO single crystal upon excitation at $\lambda_{ex} = 225$ nm. At $T = 80$ K, the PL emission spectrum is a broad complex band extending from 288 to 730 nm. At $T = 290$ K, this spectrum comprises a peak

at 413 nm (3.0 eV, FWHM = 0.83 eV) and a shoulder at 540–620 nm. Not only PL intensity increases on cooling, but the spectrum shape changes, so at 80 K the PL spectrum of the BLO crystal is dominated by two broad, partially overlapped bands with maxima at 460–477 nm and 365–375 nm.

Pustovarov et al. [11] have found that PL emission band at 371 nm (3.34 eV) is an intrinsic luminescence of BLO crystal, which arises as a result of radiative annihilation of self-trapped excitons. It is worth noting the low-temperature nature of broadband intrinsic luminescence in pristine undoped BLO crystals. The 459 nm broadband emission increases on heating from 80 to 290 K, which may indicate the presence of thermally stimulated stages in the process of PL excitation.

It is most likely that the 459 nm broadband emission at $T = 290$ K is due to unidentified lattice defects of BLO. The exact nature of these defects can not be revealed here, because of research method applied. However, it is crucial for interpretation of observed phenomena, and identification of the microscopic nature of the defects requires a separate future research. In this connection, we discuss below our idea of the origin of these defects.

Figure 9b shows the PL emission spectra recorded for BLO:Er upon excitation at $\lambda_{ex} = 258$ nm. The PL emission spectrum consists of two intense broad, partially overlapped bands at 486 and 551 nm, as well as intense PL emission band at 413 nm (3.0 eV, FWHM = 0.20 eV). We should also mention a shoulder at 653 nm and a low-intensity band in the energy region of 253–264 nm.

Figure 9c shows the PL emission spectra recorded for BLO:Nd upon excitation at $\lambda_{ex} = 264$ nm. In general, PL emission spectrum corresponds to the previous case. However, it is worth noting two important facts: the PL emission of lattice defects in BLO:Nd is less in intensity by a factor 2–2.5 in comparison with that of BLO:Er else being equal. Furthermore, the PL emission bands in BLO:Nd are somewhat shifted toward each other in comparison with those in BLO:Er.

Figure 10a shows PLE-spectra of both emission bands recorded for pristine undoped BLO crystal at $T = 80$ K. Dominant PLE-band is located at 236 nm in the spectral range of the BLO host absorption near its low-energy edge. Its low-energy slope coincides in profile with the Urbach tail of the BLO host absorption, whereas high-energy slope is determined by a decrease in the mean free path for photons in the crystal due to the increase of the optical density at the low-energy tail of the BLO host absorption. Such properties of PLE-bands are typical for both the excitonic luminescence with PL emission band at 371 nm and energy transfer through the mobile electronic excitations with PL emission band at 459–477 nm. The PLE-spectra of both bands are identical in profile at energies above $E_c' = E_c$ ($T = 80$ K). Below

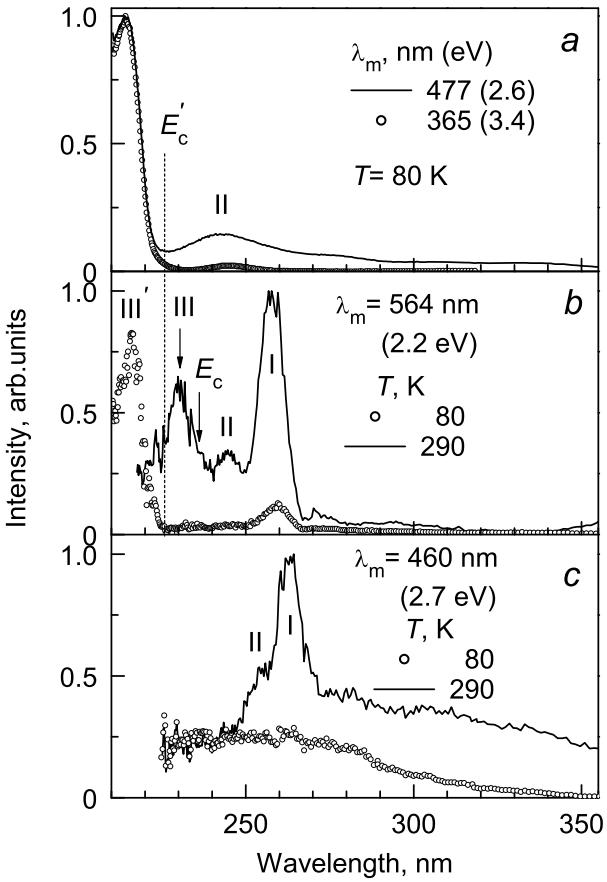

Figure 10. PL excitation spectra of lanthanum beryllate single crystals recorded monitoring emission at E_m at T = 80 or 290 K. Panel (a) shows the spectra for pristine undoped BLO crystal. Panels (b, c) demonstrate spectra for BLO crystals doped with Er^{3+} (b) or Nd^{3+} (c). Spectra of each Panel are normalized to the maximum, but they are comparable in intensity with each other within the Panel. The host absorption cutoff energies are shown for 80 (E_c') and 290 K (E_c). Roman numerals mark the relevant PLE-bands, and the symbols III and III' correspond to third PLE-band at 290 and 80 K, respectively.

E_c' (in the optical transparency band), PLE-spectrum recorded monitoring emission at 477 nm comprises low-intensity bands at 264–282 and 238–253 nm due to direct photoexcitation of defects. Excitonic luminescence ($\lambda_m = 371$ nm) has no PLE-bands in the optical transparency range, so slight intensity at 238–253 nm in PLE-spectra recorded monitoring emission at 271 nm, is due to the partial overlap of the two PL emission bands and recording high-energy tail of the other PL band at 477 nm.

Figure 10b shows PLE-spectra recorded for BLO:Er at 80 and 290 K monitoring emission at 564 nm. The spectrum comprises three PLE-bands that have been designated by Roman numerals I, II, III. At $T = 290$ K, the dominant PLE(I)-band is located at 258 nm (4.8 eV, FWHM = 0.17 eV). The PLE(II)-band is located at 245 nm, and partially overlaps with PLE(I)-band. It is about 35% in intensity

of the dominant bands. Third PLE-band is located in the energy range of the BLO host absorption and its low-energy slope coincides with the edge of the BLO host absorption. Owing to the temperature shift of the host absorption edge, location of the third PLE-band also depends on the temperature. We use the following notations for the third PLE-band: PLE(III) for $T = 290$ K and PLE(III′) for $T = 80$ K. From Fig. 10b it is evident that PLE(III)-band is a relatively low-intensity band, but it shows an energy transport to the defect by mobile electronic excitations (excitons). Upon cooling to 80-K, the PLE(I)-band intensity is about 10% of that at 290 K. The PLE(III)-band behaves inverse manner: upon cooling to 80 K, it increases in intensity and becomes dominant PLE(III′) band.

Figure 10c shows PLE-spectra recorded for BLO:Nd at 80 and 290 K monitoring emission at 459 nm. The PLE-bands (I) and (II) exhibit properties similar to those for BLO:Er. It should be noted, two important differences in PLE-spectra of BLO:Nd in comparison with those of BLO:Er. Firstly, PLE-bands (I) and (II) in BLO:Nd are lower in intensity by a factor of about 2.5 in comparison with BLO:Er. Secondly, these bands are red-shifted by 7.5–8.5 nm in comparison with those in BLO:Er. The PLE(III)-band in BLO:Nd crystals was not observed.

The PLE-spectra of BLO:Pr crystal (Fig. 8 did not show any peak which could be compared with PLE(I) band. However, the low-energy slope in the energy range of 258–270 nm is subject to a 7.5 nm red shift at room temperature. Our idea to explain these results is as follows. The BLO:Ln^{3+} emission is a superposition of the rare-earth ion emission, luminescence of the impurity related lattice defects, and intrinsic luminescence, which may dominate at low temperatures. In framework of this idea, the 302 nm emission in BLO:Pr includes not only $5d$–$4f$ emission of Pr^{3+}, but also luminescence of the lattice defects. One of the PLE-bands for the lattice defects is located in the vicinity of 258–270 nm, and excitation efficiency for this PLE band increases from 80 K to room temperature (Figs. 9, 10). The difference between the PLE spectra recorded in the vicinity of 275 nm at room temperature and 80 K (Fig. 8), is due to an increase in the contribution from the lattice defect emission at room temperature. We believe that this red shift in the BLO:Pr at 290 K is due to the advent of the new PLE-band in the spectral range of 258–270 nm. It is worth noting that this energy range corresponds exactly to the energy position of PLE(I) band in BLO:Er and BLO:Nd crystals. However, the PLE(I)-band intensity in BLO:Pr is apparently lower than that in BLO:Nd.

This allows us to discuss the overall spectroscopic picture associated with the formation of lattice defects in BLO single crystals with the introduction of trivalent impurity ions of of Er, Nd, and Pr. In our opinion, the introduction of trivalent impurity ions into BLO crystal leads to the formation of lattice defects in the vicinity of the impurity ion. Indeed, the rare earth ions doped into BLO substitute most likely La^{3+}-site and therefore there is no need for charge compensation. Probable cause of the observed lattice defect associated with trivalent impurity ion can be the difference in the ionic radii of the La^{3+} (117 pm) host ion and trivalent substitutional ions of Pr^{3+} (113 pm), Nd^{3+} (111 pm) and Er^{3+} (103 pm). The difference in ionic radii between the La^{3+} host ion and trivalent substitutional ion varies in the sequence, %: 3.4 (Pr^{3+}), 5.1 (Nd^{3+}) and 12.0 (Er^{3+}). It is pretty obvious that the change in the ionic radii occurs because of the lanthanide compression. What is surprising, the same sequence is inherent to a change in the luminescence intensity of lattice defects associated with trivalent impurity ions: the lowest intensity is observed in BLO:Pr, the highest intensity appears in BLO:Er.

4. CONCLUSIONS

Thus, the methods of optical and luminescence spectroscopy techniques were used to study the lanthanum beryllate single crystals doped with trivalent impurity ions of Er, Nd, or Pr. Trivalent impurity ions of Ln^{3+} (Ln= Er, Nd, or Pr) were introduced into the lattice of BLO single crystals during the growth process. The most likely place for the localization of these impurity ions is the position of the La3+ host ion. The main conclusions of the research work are as follows.

1. The introduction of trivalent impurity ions of Ln^{3+} leads to the following location of $4f$ ground states regarding the energy levels of BLO single crystal: $4f^2$ level of Pr^{3+} ion ($^3H_4$) is located in the band gap at 1 eV above the VB top; $4f^3$ level of Nd^{3+} ion ($^4I_{9/2}$) and $4f^{11}$ level of Er^{3+} ion ($^4I_{15/2}$) are located in the valence band at 0.36 eV (Nd^{3+}) and 1.26 eV (Er^{3+}) below the VB top.

2. Intraconfigurational $4f$–$4f$ transitions in BLO:Ln single crystal can occur from $4f^n$ ground level of Ln^{3+} onto highly excited $4f$-states up to ^3P_J, $^1I_6$ (Pr^{3+}), $^2F2_{7/2}$ (Nd^{3+}), and $^4D_{3/2}$ (Er^{3+}) states. The $^1S_0$ state of Pr^{3+} ion is located in energy by 1.5 eV above the $5d\,4f^1$ level, and the expected energy of the $^3H_4 \rightarrow {}^1S_0$ transition lies in the energy range of the BLO host absorption.

3. Interconfigurational $4f$–$5d$ transitions in BLO:Ln single crystals are possible only for Pr^{3+} ion ($E_{fd} = 4.5$–4.8 eV). The energy thresholds of $4f$–$5d$ transitions for Nd^{3+} and Er^{3+} ions are located in the energy range of the BLO host absorption.

4. The threshold energy of charge-transfer transitions O–Ln^{3+} for all three considered Ln^{3+} ions (Ln= Er, Nd, Pr) are located in the energy range of the BLO host absorption.

5. Lattice defects are responsible for the appearance of additional PL emission bands in the spectral range of 413–620 nm, with appropriate PLE-bands in the UV-spectral region. The exact spectral location and intensity of the PLE-bands vary somewhat depending on the impurity ion. The trend of increase in PL intensity of these defects in the sequence of the Pr–Nd–Er impurity ions was revealed.

ACKNOWLEDGMENTS

The authors are grateful to V.N. Matrosov for providing samples for examination and A.A. Maslakov for assistance in the spectroscopic measurements. This work was partially supported by the Ministry of Education and Science, Russia (the basic part of the government mandate), Center of Excellence "Radiation and Nuclear Technologies" (Competitiveness Enhancement Program of Ural Federal University, Russia), HASYLAB DESY (Projects Nos. 20110843, 20080119EC).

REFERENCES

1. Y.K. Voronko, G.V. Maksimova, V.V. Osiko, A.A. Sobol, B.P. Starikov, and M.I. Timoshechkin, Phys. Status Solidi A **17**, K41 (1973).
2. R.C. Morris, C.F. Cline, R.F. Begley, M. Dutoit, P.J. Harget, H.P. Jenssen, T.S. LaFrance, and R. Webb, Appl. Phys. Lett. **27**, 444 (1975).
3. H.P. Jenssen, R.F. Begley, R. Webb, and R.C. Morris, J. Appl. Phys. **47**, 1496 (1976).
4. A.A. Kaminskii, T. Ngoc, S.E. Sarkisov, V.N. Matrosov, and M.I. Timoshechkin, Phys. Status Solidi A **59**, 121 (1980).
5. A.W. Tucker, M. Birnbaum, and C.L. Fincher, J. Appl. Phys. **52**, 3067 (1981).
6. A.W. Tucker, M. Birnbaum, and C.L. Fincher, J. Appl. Phys. **52**, 5434 (1981).
7. R. Scheps, Appl. Opt. **28**, 89 (1989).
8. L.A. Harris and H.L. Yakel, Acta Crystallogr. B **24**, 672 (1968).
9. T.A. Betenekova, A.V. Kruzhalov, N.M. Osipova, V.P. Palvanov, V.L. Petrov, and I.N. Shabanova, Sov. Phys. Solid State **25**, 95 (1983).
10. A.V. Kruzhalov, V.A. Pustovarov, A.A. Maslakov, V.L. Petrov, and B.V. Shulgin, Opt. Spectrosc. **63**, 268 (1987).
11. V.A. Pustovarov, V.L. Petrov, E.I. Zinin, M. Kirm, G. Zimmerer, and B.V. Shulgin, Phys. Solid State **42**, 253 (2000).
12. A.V. Kruzhalov, A.A. Maslakov, V.L. Petrov, and B.V. Shulgin, Zh. Prikl. Spektrosk. **45**, 859 (1986).
13. D.M. Gualtieri, J. Luminesc. **60–61**, 127 (1994).
14. N.V. Kuleshov, A.S. Shinkevich, V.G. Shcherbitsky, V.P. Mikhailov, T. Danger, T. Sandrock, and G. Huber, Opt. Mater. **5**, 111 (1996).
15. S. Mahlik, M. Malinowski, and M. Grinberg, Opt. Mater. **34**, 164 (2011).
16. R. Piramidowicz, M. Kowalska, and M. Malinowski, J. Alloys Compd. **300–301**, 430 (2000).
17. V. Sudesh, J.A. Piper, E.M. Goldys, and R.S. Seymour, J. Opt. Soc. Am. B: Opt. Phys. **15**, 239 (1998).
18. J.B. Czirr and M. Berrondo, US Patent No. 5483062 (1996).
19. V.A. Pustovarov, I.N. Ogorodnikov, and E.A. Ospanbekov, J. Opt. Soc. Am. B: Opt. Phys. **32**, 241 (2015).
20. I.N. Ogorodnikov and V.A. Pustovarov, J. Luminesc. **9**(6), 1176 (2015).
21. P. Dorenbos, J. Luminesc. **122–123**, 315 (2007).
22. E.G. Tsvetkov, G.M. Rylov, and V.N. Matrosov, Mater. Res. Bull. **41**, 307 (2006).
23. G. Zimmerer, Rad. Meas. **42**, 859 (2007).
24. G.H. Dieke, *Spectra and Energy Levels of Rare Earth Ions in Crystals* (Wiley Interscience, New York, 1968).
25. R.T. Wegh, A. Meijerink, R.-J. Lamminmäki, and J. Hölsä, J. Luminesc. **87–89**, 1002 (2000).
26. A.J. Wojtowicz and M. Malinowski, in *HASYLAB Annual Report* (Hamburg, 1999), p. 277.
27. V.A. Pustovarov, in *Proceedings of the 17th International Conference on Luminescence and Optical Spectroscopy of Condensed Matter, Wrozlaw, 2014*, p. 227.
28. R. Shendrik and E. Radzhabov, IEEE Trans. Nucl. Sci. **57**, 1295 (2010).
29. V.N. Makhov, N.M. Khaidukov, N.Yu. Kirikova, M. Kirm, J.C. Krupa, T.V. Ouvarova, and G. Zimmerer, J. Luminesc. **87–89**, 1005 (2000).